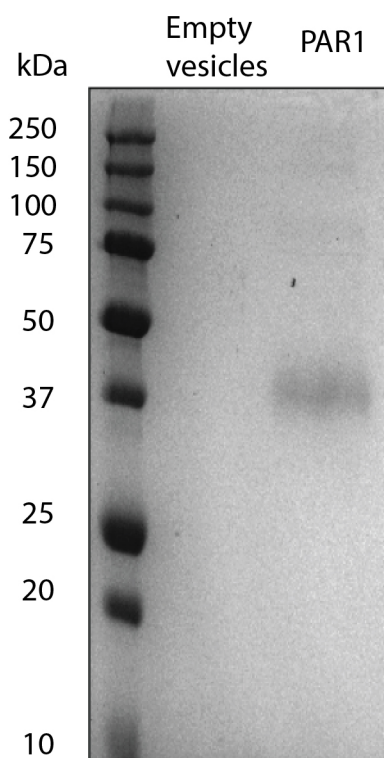


Supplementary Figure 1

Principle of force-distance (FD) curve-based AFM.

(a) FD-based AFM contours the sample surface while oscillating the AFM tip with a sine wave at a frequency of 0.25 kHz. Pixel-by-pixel the AFM tip is approached (blue curve) and retracted (red curve) from the sample. The AFM cantilever deflection measures the force interacting between AFM tip and sample. During these approach and retraction cycles the force vs time (b) and force vs distance (c) is recorded. Thereby, the maximal force (imaging force) used to touch the sample F_i is kept constant using a feedback loop. (c) The mechanical deformation or distance of deformation D_{Def} of a soft biological sample is described by the indentation of a much stiffer AFM tip. This indentation is detected at a certain repulsive force. (d) During retraction, adhesive force F_{Adh} is recorded between the tip and the sample. Using a functionalized cantilever F_{Adh} can detect the rupture of specific interactions between for example a functionalized tip and sample. (e) The parameters extracted from individual force curves can be displayed as maps such as the sample topography (height image) contoured at a given imaging force, the adhesion force or sample deformation¹.

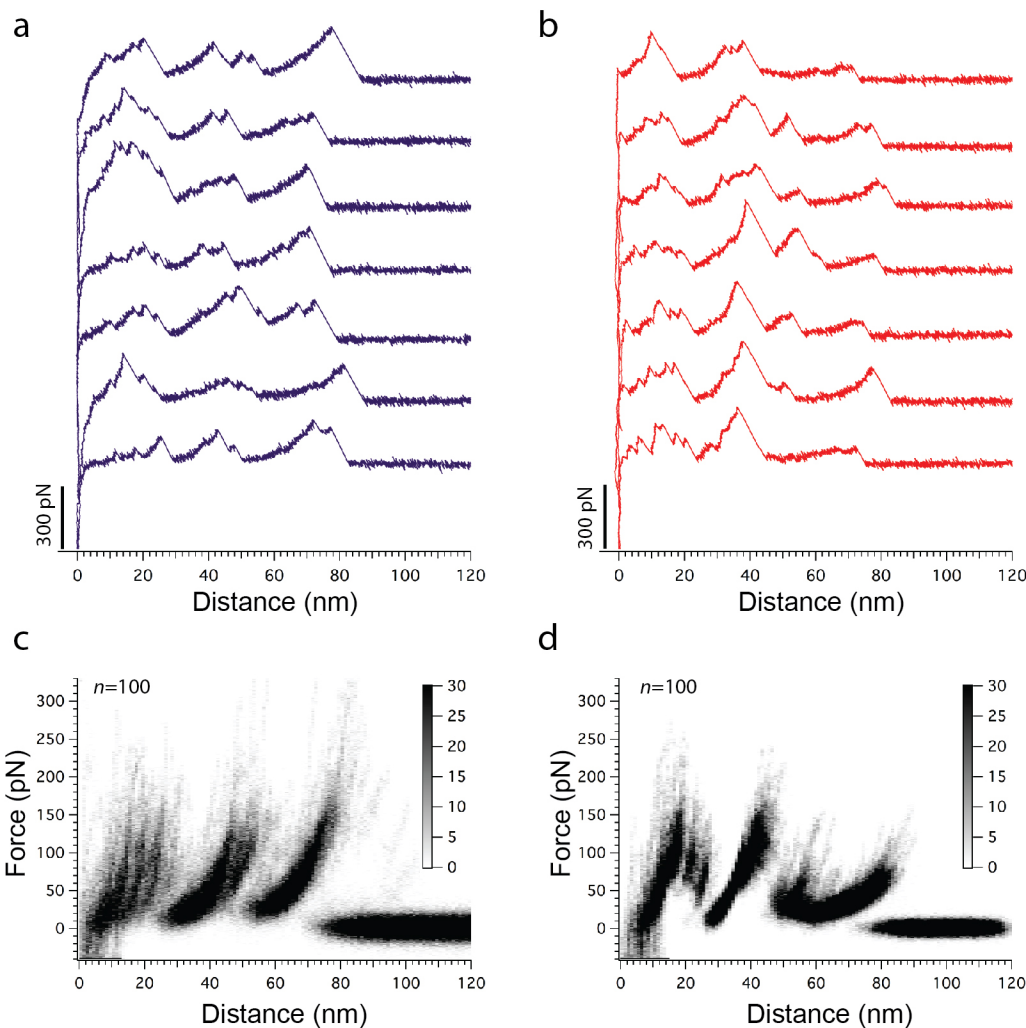
1. Medalsy, I., Hensen, U. & Muller, D.J. Imaging and quantifying chemical and physical properties of native proteins at molecular resolution by force-volume AFM. *Angew Chem Int Ed Engl* **50**, 12103-12108 (2011).



Supplementary Figure 2

SDS-PAGE of PAR1 liposomes.

SDS-PAGE was performed on a 12% acrylamide gel with 150 V and 60 min in a loading buffer (50 mM Tris, pH 7, 6% SDS, 50 mM DTT, 8% glycerol, 0.1% bromphenol blue) and stained with Coomassie blue. Lane 1, molecular weight marker; Lane 2, 10 μ L of empty lipid vesicles (liposomes made of 0.5 mg mL⁻¹ DOPC and 0.05 mg mL⁻¹ CHS); Lane 3, 10 μ L of PAR1 proteoliposomes (10 μ M PAR1 reconstituted in liposomes made of 0.5 mg mL⁻¹ DOPC and 0.05 mg mL⁻¹ CHS). The band at \approx 40 kDa is in good agreement with the expected size of 43.9 kDa calculated from the PAR1 sequence.

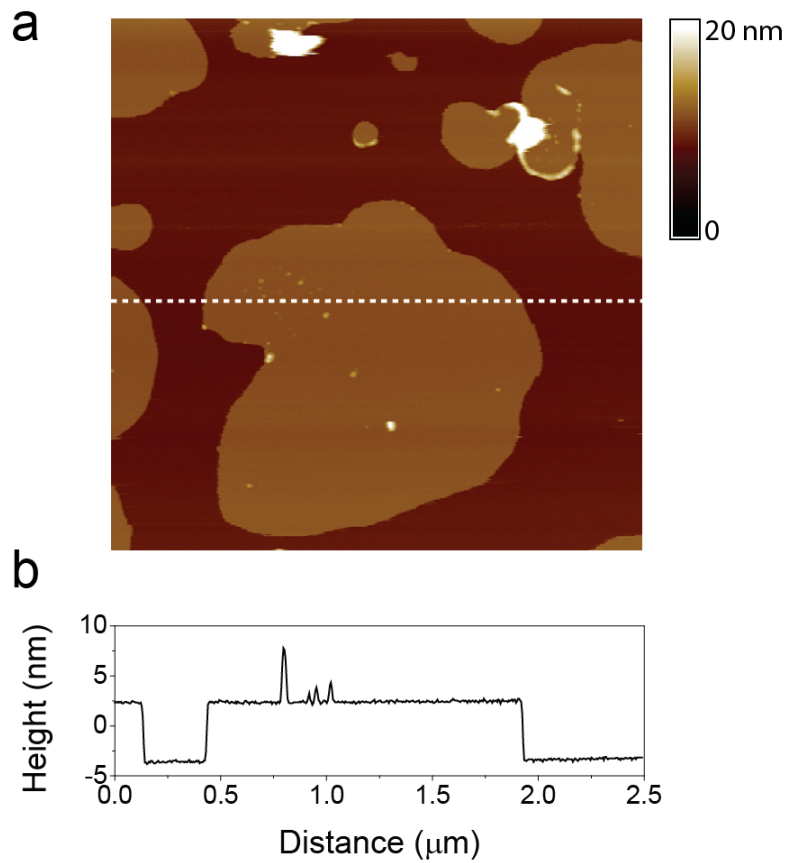


Supplementary Figure 3

SMFS of human PAR1 and human β_2 AR reconstituted in liposomes.

Selection of FD curves of recorded upon unfolding of single PAR1 (a) and β_2 AR (b) embedded in lipid membranes composed of DOPC and CHS. Superimpositions of FD curves recorded of PAR1 (c) and β_2 AR (d)^{2,3}. For each GPCR the FD curves recorded were superimposed following the procedure previously described for β_2 AR^{3,4}. n gives the number of FD curves superimposed. For SMFS, PAR1 proteoliposomes were adsorbed for 1 h at room temperature to freshly cleaved mica in SMFS buffer solution (300 mM NaCl, 25 mM MgCl₂, 25 mM Tris, pH 7.0) and β_2 AR proteoliposomes were adsorbed over night at 4°C to freshly cleaved mica in SMFS buffer solution. It has been shown that the stability of human and animal GPCRs embedded in lipid membranes and adsorbed onto mica in buffer solution does not alter within 24 h³⁻⁵. Thus, samples were newly prepared before becoming 24 h old. Within this 24 h time frame we could not observe any alteration of the FD curves, which would indicate denaturation of the GPCR. For each GPCR characterized by SMFS we had to prepare at least 20 different samples. Each time a new sample has been prepared a new AFM cantilever was taken. SMFS of both GPCRs was conducted as described³ and carried out using automated AFM-based SMFS (ForceRobot 300; JPK Instruments)². SMFS data of both β_2 AR and PAR1 were recorded in SMFS buffer solution, at room temperature and at pulling velocities of 300-900 nm s⁻¹.

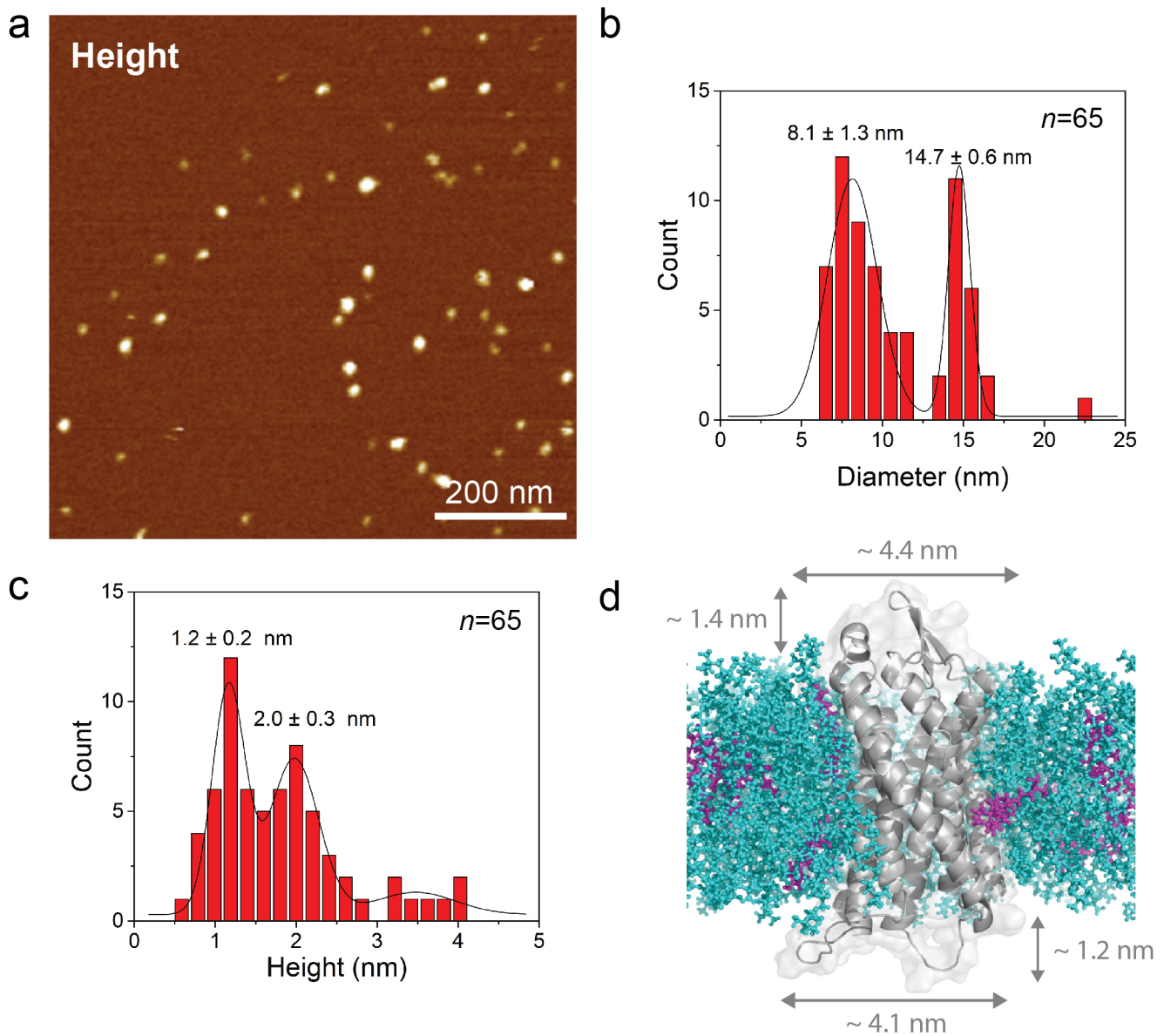
2. Struckmeier, J. et al. Fully automated single-molecule force spectroscopy for screening applications. *Nanotechnology* **19**, 384020 (2008).
3. Zocher, M., Fung, J.J., Kobilka, B.K. & Muller, D.J. Ligand-specific interactions modulate kinetic, energetic, and mechanical properties of the human beta2 adrenergic receptor. *Structure* **20**, 1391-1402 (2012).
4. Zocher, M., Zhang, C., Rasmussen, S.G., Kobilka, B.K. & Muller, D.J. Cholesterol increases kinetic, energetic, and mechanical stability of the human beta2-adrenergic receptor. *Proc Natl Acad Sci U S A* **109**, E3463-3472 (2012).
5. Saprà, K.T. et al. Detecting molecular interactions that stabilize bovine rhodopsin. *J Mol Biol* **358**, 255-269 (2006).



Supplementary Figure 4

Overview AFM topograph of PAR1 proteoliposome.

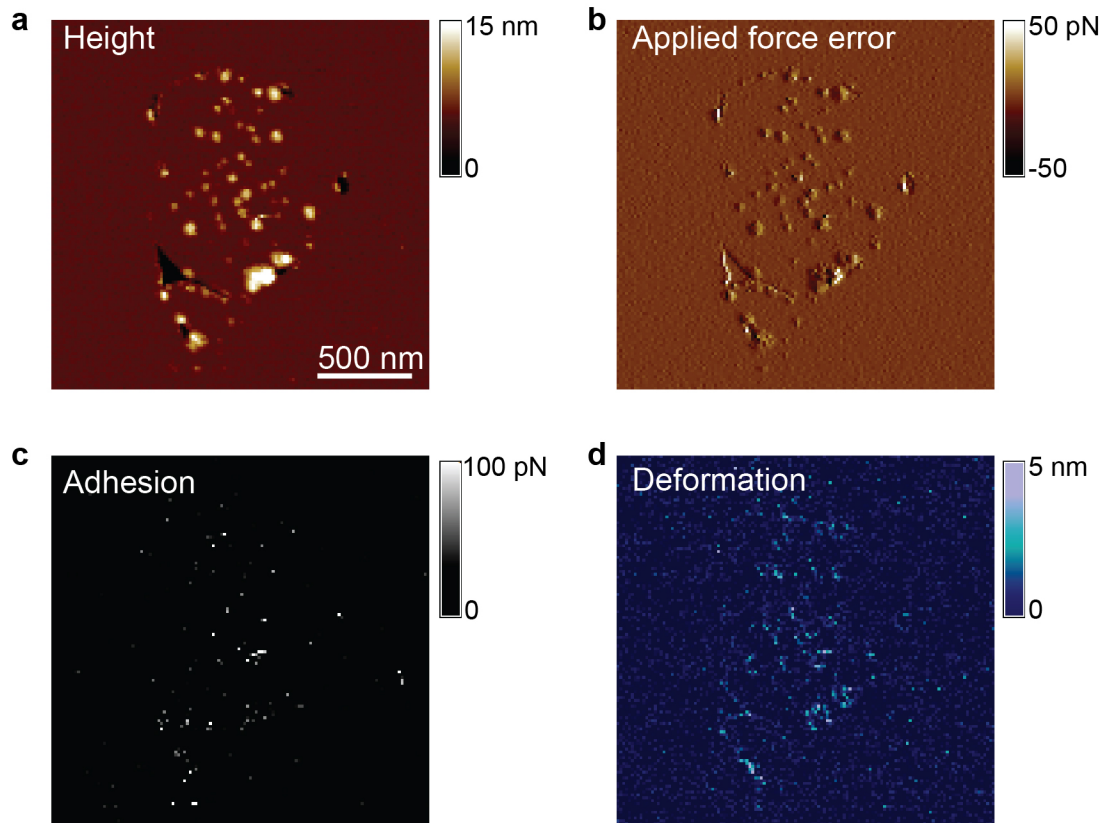
(a) Topography (height image, $2.5 \times 2.5 \mu\text{m}^2$) showing membrane patches on mica. Proteoliposomes were adsorbed to freshly cleaved mica in buffer solution. To remove weakly attached membrane patches, the sample was rinsed several times with the buffer (see **Online Methods**). After adsorption to mica the proteoliposomes break open so that they showed single-layered membrane patches. (b) Cross-section (white dashed line in (a)) showing a lipid membrane protruding $4.5 \pm 0.7 \text{ nm}$ (average \pm S.D., $n=10$) from the supporting mica. The sparsely distributed single protrusions originating from single or clustered PAR1. The FD-based AFM topograph was recorded in imaging buffer (300 mM NaCl, 20 mM HEPES, 25 mM MgCl₂, pH 7.0) at room temperature.



Supplementary Figure 5

Structural analysis of PAR1 reconstituted in proteoliposomes.

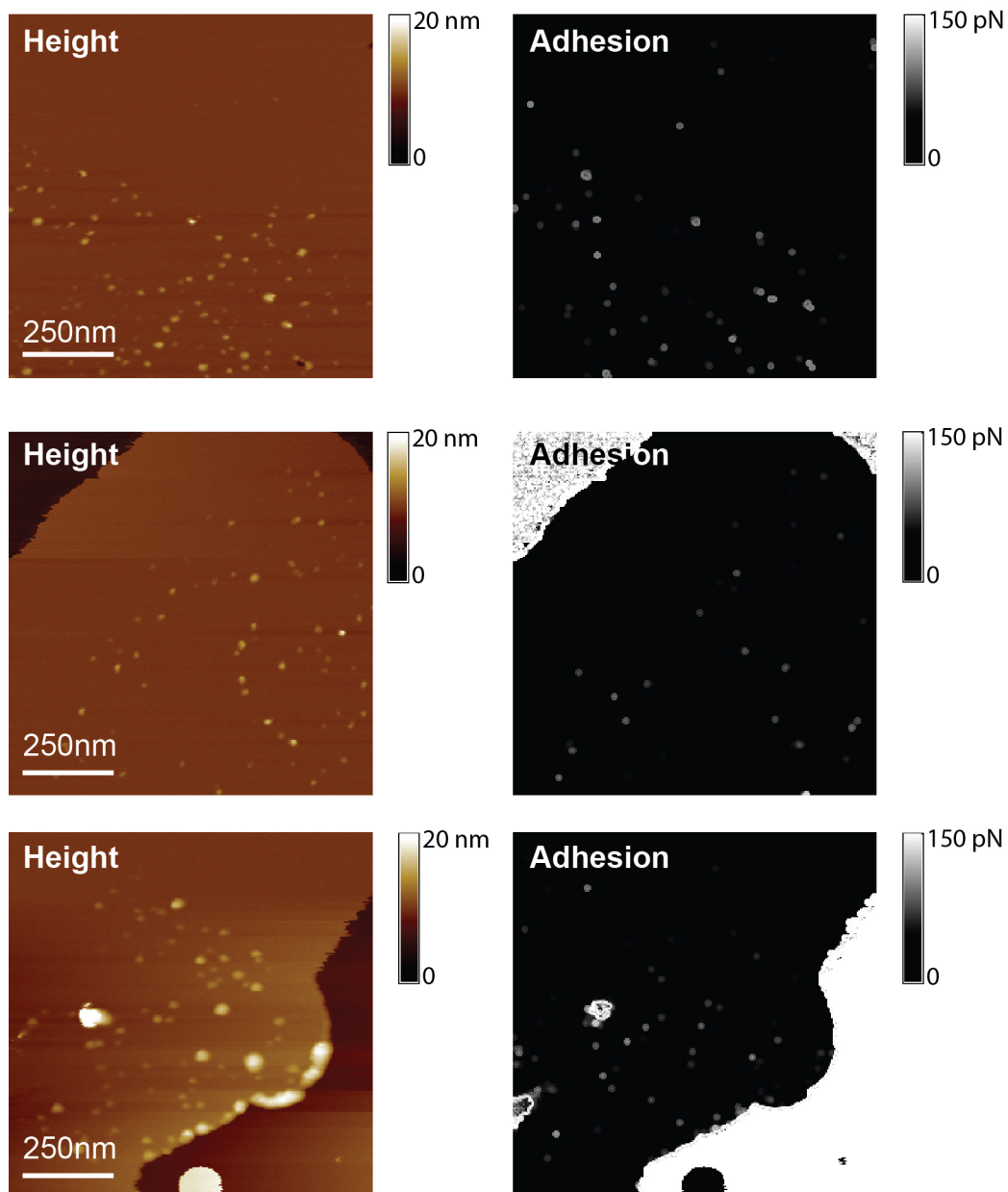
(a) Topography of PAR1s sparsely distributed in lipid membranes made of 0.5 mg mL^{-1} DOPC and 0.05 mg mL^{-1} CHS. Histogram of diameter (b) and height (c) of PAR1 particles imaged in (a). (b) The diameter distribution showed two peaks centered at $8.1 \pm 1.3 \text{ nm}$ (average \pm S.D.) and $14.7 \pm 0.6 \text{ nm}$. Diameters were measured at full-width half maximum of particle heights. (c) The height distribution showed two peaks centered at $1.2 \pm 0.2 \text{ nm}$ (average \pm S.D.) and $2.0 \pm 0.3 \text{ nm}$, which could correspond to the height of the extracellular or intracellular surface emerging from the DOPS/CHS membrane, respectively (d). The FD-based AFM topograph was recorded in imaging buffer (300 mM NaCl , 20 mM Hepes , 25 mM MgCl_2 , $\text{pH } 7.0$) at room temperature. n gives the number of PAR1 particles analyzed.



Supplementary Figure 6

AFM topograph and multiparametric maps of PAR1 reconstituted in liposomes.

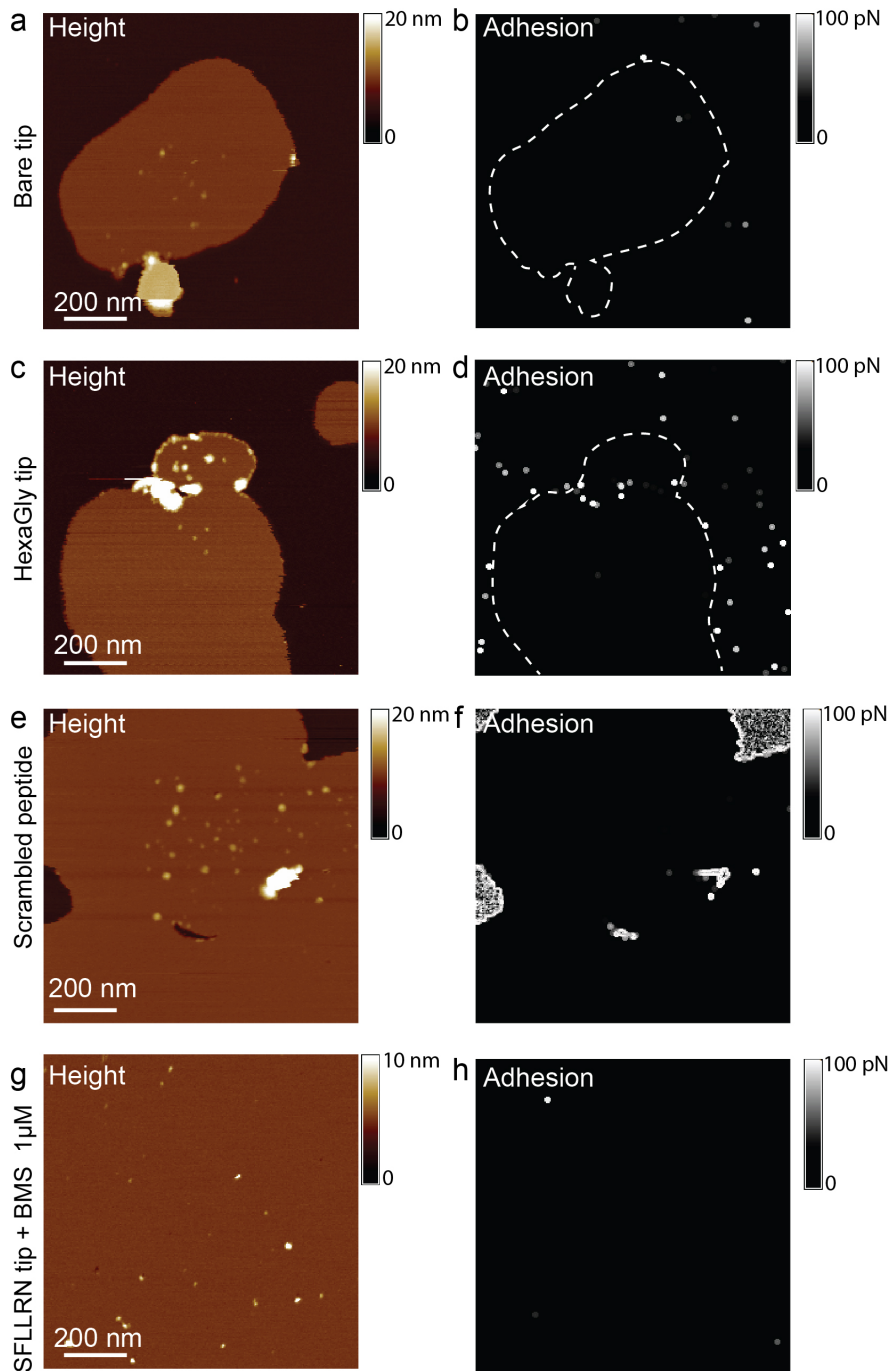
(a) Topograph showing single and clustered PAR1 molecules protruding from the lipid bilayer. (b) Applied force error map showing low errors of <20 pN. (c) Adhesion map showing the SFLLRN functionalized AFM tip interacting sparsely with the lipid bilayer and mainly with PAR1 (see (a)). (d) Deformation map showing enhanced deformation values of PAR1 molecules. The FD-based AFM data was recorded as described (**Online Methods**).



Supplementary Figure 7

Mapping the binding of the SLLRN ligand to human PAR1 proteoliposomes using FD-based AFM.

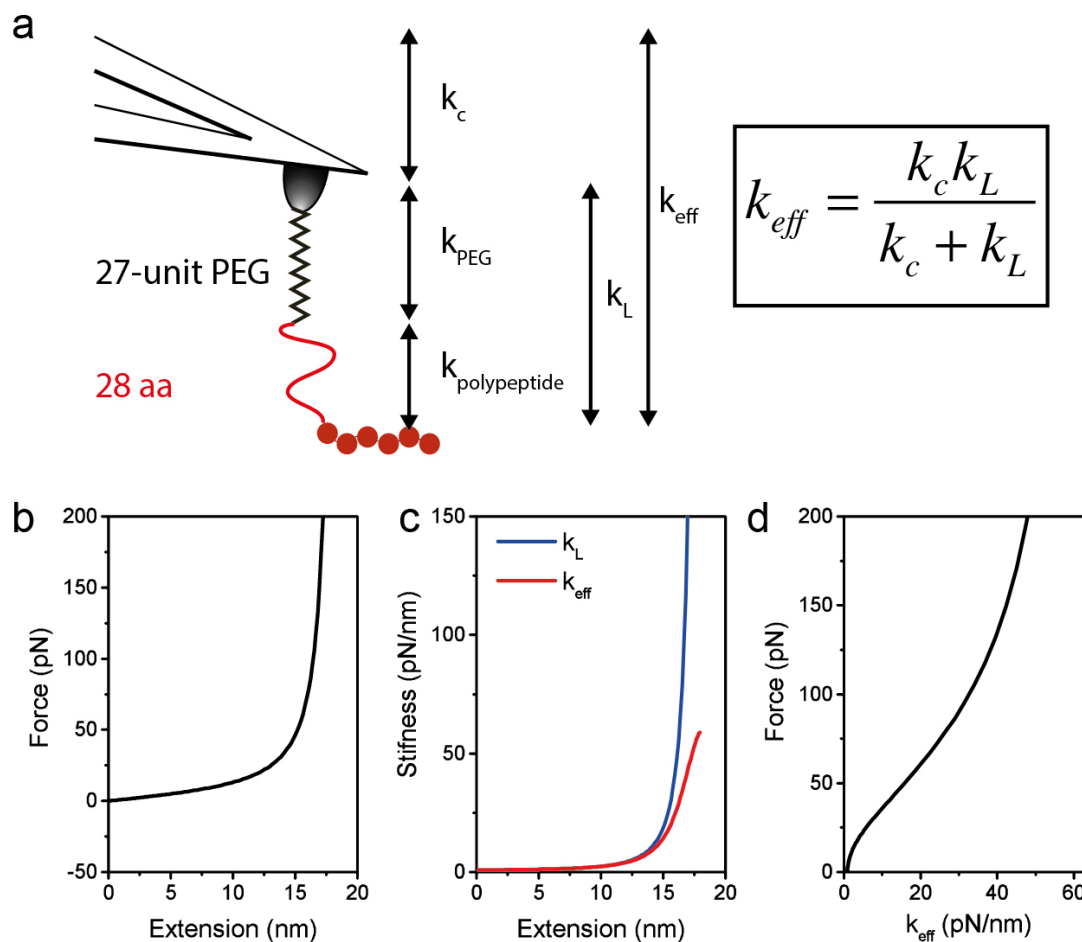
Topographs (left column) of human PAR1 reconstituted in proteoliposomes taken with the SLLRN-ligand functionalized AFM tip oscillated at 0.25 kHz and amplitude of 50 nm. As described, the SLLRN has been attached *via* the PEG-polypeptide linker to the AFM tip (**Fig. 1c**). Corresponding adhesion maps (right column). To increase their visibility adhesive pixel were enlarged by a factor 2. The FD-based AFM data was recorded as described (**Online Methods**).



Supplementary Figure 8

Validating that SFLLRN ligand-functionalized AFM tips detect specific interactions with PAR1.

Height images (a,c,e,g) and corresponding adhesion images (b,d,e,h) recorded with either (a,b) a bare AFM tip, (c,d) a hexa-glycine, (e,f) a scrambled peptide (FLLNSR) or (g,h) a SFLLRN functionalized tip in the presence of peptide mimetic antagonist (1 μM BMS). Every functional group (hexa-glycine, FLLNSR, or SFLLRN) was attached *via* the same PEG-polypeptide linker to the AFM tip (Fig. 1c). This supplementary figure correlates to Fig. 2, which maps receptor-ligand interactions on PAR1 using SFLLRN functionalized AFM tips. The FD-based AFM data was recorded as described (Online Methods).



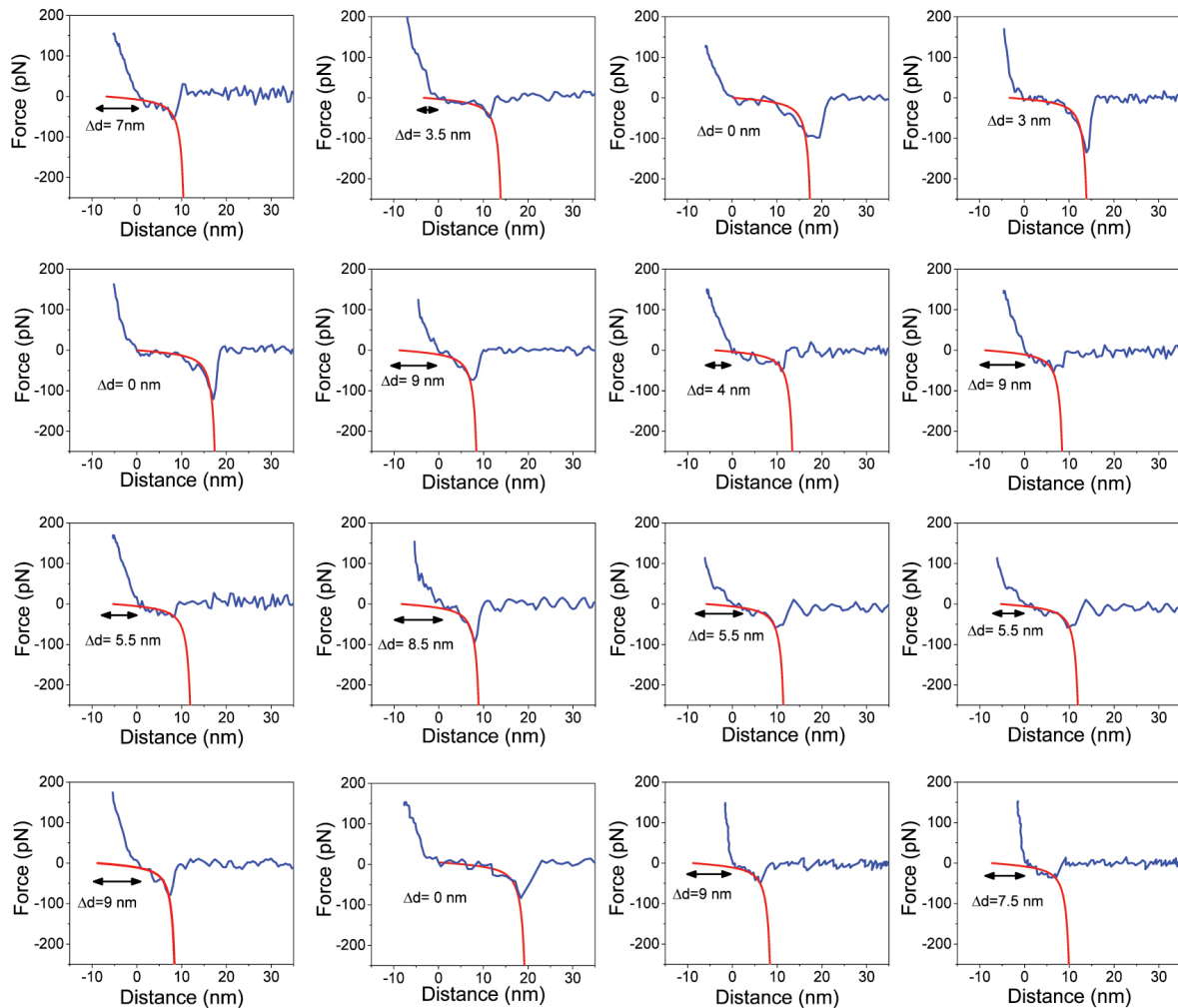
Supplementary Figure 9

Determining the effective spring constant k_{eff} of the cantilever-PEG-polypeptide linker system.

(a) The effective spring constant k_{eff} is the combination of the cantilever stiffness k_c and the stiffness k_L of the PEG-polypeptide linker. As described (Supplementary Note), k_L was estimated using the combination of the elasticity of the PEG linker (k_{PEG}) and the elasticity of the polypeptide linker ($k_{polypeptide}$). The linker consists of the 27-unit long PEG spacer and the 28 aa long polypeptide, which mimics the thrombin cleaved N-terminal end of PAR1 (comp. **Fig. 1**). (b) The extension of the PEG-polypeptide linker applied to a stretching force F in water is described by the combination of both the PEG elasticity model⁶ and the WLC model⁷. (c) Calculated stiffness k_L of the PEG-polypeptide linker (blue curve) vs extension and effective stiffness k_{eff} of cantilever and linker (red curve). (d) The force vs k_{eff} relationship was used to determine the effective spring constant of cantilever-PEG-polypeptide linker system exposed to a given force F_{eq} and to subsequently calculate ΔG_{bu} .

6. Sulchek, T., Friddle, R.W. & Noy, A. Strength of multiple parallel biological bonds. *Biophys. J.* **90**, 4686-4691 (2006).

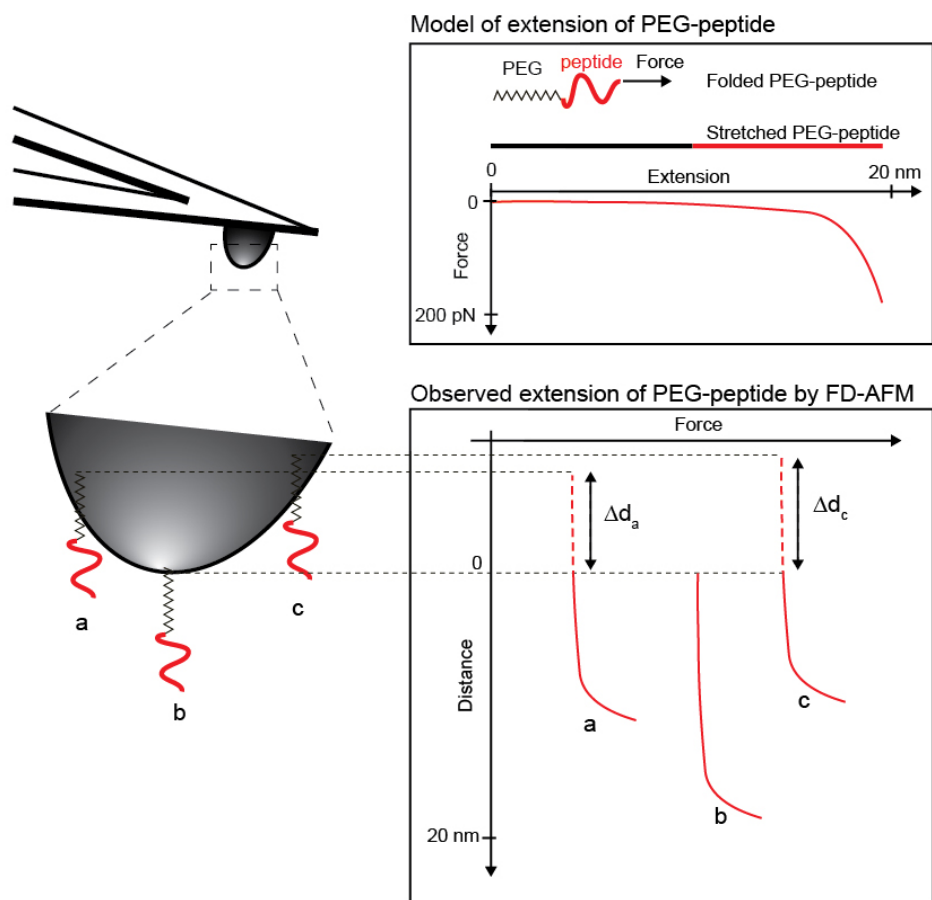
7. Bustamante, C., Marko, J.F., Siggia, E.D. & Smith, S. Entropic elasticity of lambda-phage DNA. *Science* **265**, 1599-1600 (1994).



Supplementary Figure 10

Validating the elastic potential of the PEG-polypeptide linker attaching the ligand to the AFM tip.

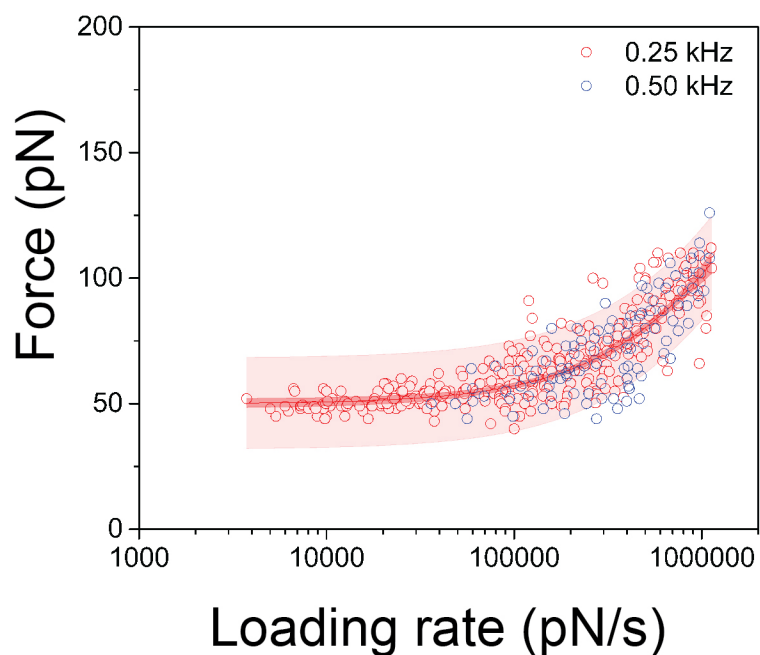
Shown are individual FD curves, each one detecting the rupture of a specific SFLLRN-PAR1 bond. Each of these representative FD curves was fitted using the effective spring constant k_{eff} of the cantilever-PEG-polypeptide linker system (**Supplementary Fig. 9**). The individual fits were shifted along the distance axis to minimize the sum of squared residuals between the fit and the adhesion force peak. The Δd values given correspond to the shifted distance. FD curves were recorded as described (**Fig. 2**) using a SFLLRN functionalized AFM cantilever and imaging a PAR1 proteoliposome by FD-based AFM.



Supplementary Figure 11

The position of the PEG-polypeptide linker bound to the tip affects the distance of the force peak stretching the linker.

The stretching of the PEG-polypeptide linker under force is described combining the model describing the PEG elasticity and the WLC model describing the polypeptide elasticity (see Supplementary Note). Independent of the position at which the PEG-polypeptide linker is chemically anchored to the AFM tip the force-distance characteristics describing the stretching of the linker is always similar since in all cases the linker is bound via one terminal end to the AFM tip and with the other terminal end adheres to the receptor. However, due to the vertical position at which the linker is anchored to the tip, the first part of the force-distance characteristics describing the stretching of the PEG-polypeptide linker can be hidden by relative distance " Δd " value (dashed line).



Supplementary Figure 12

Influence of the AFM tip drive frequency on ligand-receptor unbinding force.

DFS plot showing that the tip drive frequency (0.25 kHz, red or 0.5 kHz, blue) has no influence on the force required to separate SFLLRN-ligand and PAR1. Although the higher oscillation frequency reduced the contact time between tip and sample and, thus, lowered the frequency of bonds formed between ligand and PAR1, we could record a sufficient amount of specific unbinding events. Data were recorded in imaging buffer (300 mM NaCl, 20 mM Hepes, 25 mM MgCl₂, pH 7.0) at room temperature and fitted using the Friddle-Noy-de Yoreo model (thin red line)⁸. Each circle represents one measurement. Darker red shaded areas represent 99% confidence intervals and lighter red shaded areas represent 99% of prediction intervals.

8. Friddle, R.W., Noy, A. & De Yoreo, J.J. Interpreting the widespread nonlinear force spectra of intermolecular bonds. *Proc Natl Acad Sci U S A* **109**, 13573-13578 (2012).

Supplementary Information

Supplementary note

Establishing a realistic measure of the elastic potential and experimental fit

To establish a direct connection between F_{eq} and ΔG_{bu} , we need to establish a realistic measure of the elastic potential $E_s(F_{\text{eq}})$ of the linker tethering the hexa-amino acid sequence (e.g., SFLLRN or other) to the AFM tip. This linker consists of a 27-unit PEG spacer and a 28 aa long polypeptide, which mimics the thrombin cleaved native N-terminal end of PAR1 (**Fig. 1c** and **Supplementary Fig. 9a**). To properly describe the entire PEG-polypeptide linker, we depicted the extension of polypeptide using the worm-like-chain (WLC) model¹ (with a persistence length of $l_p = 0.4$ nm and a contour length of $L_c = 28$ aa) and the extension of the PEG spacer containing 27 monomers (n_m) in water² using the model for PEG elasticity² (with a Kuhn length of $L_k = 0.7$ nm, a segment elasticity of $K_s = 150$ N/m, a monomer length in planar configuration of $L_{\text{planar}} = 0.358$ nm, a monomer length in helical configuration of $L_{\text{helical}} = 0.28$ nm and a free energy difference between planar and helical configuration of $\Delta G = 3 k_bT$).

Worm-like-chain model:

$$F = \frac{k_bT}{l_p} \left(\frac{1}{4 \left(1 - \frac{x}{L_c}\right)^2} + \frac{x}{L_c} - 0.25 \right)$$

Model for PEG elasticity:

$$L(F) = L_c(F) \times \left(\coth\left(\frac{Fl_k}{k_bT}\right) - \frac{k_bT}{Fl_k} \right) + \frac{n_m F}{K_s}$$
$$L_c(F) = n_m \times \left(\frac{L_{\text{planar}}}{e^{\frac{\Delta G(F)}{k_bT}} + 1} + \frac{L_{\text{helical}}}{e^{-\frac{\Delta G(F)}{k_bT}} + 1} \right)$$
$$\Delta G(F) = \Delta G - F(L_{\text{planar}} - L_{\text{helical}})$$

Combining both models, we obtained the force-extension relationship of the PEG-polypeptide linker (**Supplementary Fig. 9b**). Derivative of this force-extension relationship results in the stiffness-extension k_L of the entire linker (**Supplementary Fig. 9c**, blue curve). Finally, using the relationship for two springs in series (cantilever spring k_c and linker spring k_L) (**Supplementary Fig. 9a**), we obtained the stiffness k_{eff} of the cantilever-PEG-polypeptide system (**Supplementary Fig. 9c**, red curve).

After having established a more realistic measure of the elastic potential stressing the ligand-receptor bond we applied this relationship to fit unbinding (or

adhesion) events recorded in single force-distance (FD) curves. As shown in **Supplementary Fig. 10** this relationship describes very well the specific adhesion events. Thereby, every unbinding event is fitted using the same fitting parameters and the fitted curves were simply shifted along the distance axis by Δd . As explained schematically in **Supplementary Fig. 11**, this Δd -value refers to the vertical distance between the tip apex and the position at which the linker chemically anchored to the tip. As shown in the schematics, a linker anchored by a distance Δd above the tip apex will lead to the hiding of the first Δd of the model curve fit. Analyzing the specific unbinding events detected in FD curves, which were recorded with the same functionalized AFM tip, in average showed 1–3 different Δd values. This suggests that an average AFM tip only bears a few functional groups at the tip apex. These Δd values were in the range of 0–12 nm, which is compatible with the expected length of the PEG-polypeptide linker. Therefore, we validate the above-mentioned model to realistically describe the elastic potential of the PEG-polypeptide linker.

Supplementary Table 1 | Overview of peptides probed for their specific binding to PAR1.

Peptide	Inhibition	Parameters extracted from DFS plots			ΔG_{bu} (kcal/mol)	K_d	Affinity	Data shown in
		F_{eq} (pN)	x_u (Å)	k_{off}^0 (s ⁻¹)				
SFLLRN	--	49.9 ± 0.9	0.6 ± 0.2	3621 ± 885	-11.22 ± 0.42	≈350 nM	High	Fig. 4
	BMS	--	--	--	--	--	None	Supp. Fig. 8
	Vorapaxar	26.4 ± 1.6	0.3 ± 0.1	6930 ± 450	-8.38 ± 1.04	≈40 μM	Low	Fig. 4
SFLLAN	--	29.5 ± 1.4	0.6 ± 0.2	2767 ± 361	-8.61 ± 0.82	≈30 μM	Low	Fig. 4
	Vorapaxar	27.1 ± 1.8	0.3 ± 0.2	6002 ± 398	-8.47 ± 1.12	≈35 μM	Low	Fig. 4
SALLRN	--	14.1 ± 4.7	0.3 ± 0.1	4079 ± 1302	-5.73 ± 3.67	≈3500 μM	None	Fig. 4
A(pF-F)RChahRY	--	51.1 ± 1.3	0.6 ± 0.1	3212 ± 370	-11.77 ± 0.58	≈100 nM	High	Fig. 4
FLNSR (scrambled)	--	--	--	--	--	--	None	Supp. Fig. 8
GGGGGG	--	--	--	--	--	--	None	Supp. Fig. 8

Supplementary References

1. Bustamante, C., Marko, J.F., Siggia, E.D. & Smith, S. Entropic elasticity of lambda-phage DNA. *Science* **265**, 1599-1600 (1994).
2. Sulchek, T., Friddle, R.W. & Noy, A. Strength of multiple parallel biological bonds. *Biophys. J.* **90**, 4686-4691 (2006).